# A systematic development of a polarizable potential of water

Péter T. Kiss and András Baranyai

Citation: J. Chem. Phys. **138**, 204507 (2013); doi: 10.1063/1.4807600
View online: http://dx.doi.org/10.1063/1.4807600
View Table of Contents: http://jcp.aip.org/resource/1/JCPSA6/v138/i20
Published by the American Institute of Physics.

# A systematic development of a polarizable potential of water

Péter T. Kiss and András Baranyai
*Institute of Chemistry, Eötvös University, P.O. Box 32, 1518 Budapest 112, Hungary*

(Received 10 December 2012; accepted 8 May 2013; published online 31 May 2013)

Based on extensive studies of existing potentials we propose a new molecular model for water. The new model is rigid and contains three Gaussian charges. Contrary to other models, all charges take part in the polarization of the molecule. They are connected by harmonic springs to their gas-phase positions: the negative charge to a prescribed point on the main axis of the molecule; the positive charges to the hydrogens. The mechanical equilibrium between the electrostatic forces and the spring forces determines the polarization of the molecule which is established by iteration at every timestep. The model gives excellent estimates for ambient liquid properties and reasonably good results from high-pressure solids to gas-phase clusters. We present a detailed description of the development of this model and a large number of calculated properties compared to the estimates of the non-polarizable TIP4P/2005 [J. L. F. Abascal and C. Vega, J. Chem. Phys. **123**, 234505 (2005)], the polarizable GCPM [P. Paricaud, M. Predota, A. A. Chialvo, and P. T. Cummings, J. Chem. Phys. **122**, 244511 (2005)], and our earlier BKd3 model [P. T. Kiss and A. Baranyai, J. Chem. Phys. **137**, 084506 (2012)]. The best overall performance is shown by the new model. © *2013 AIP Publishing LLC*. [http://dx.doi.org/10.1063/1.4807600]

## I. INTRODUCTION

In the past four decades several dozen molecular models of water have been suggested and tested as simple entities capable of mimicking water as a bulk liquid, solid, or vapor using only classical mechanics and electrostatics.[1,2] During this time the scientific community gradually canonized several models as easy to use, computationally cost-effective force fields, and applied them for many different problems. The most notable models in this sense are the SPC/E,[3] the TIP4P,[4] and the TIP3P[4] models. These are rigid, nonpolarizable models fitted to the properties of ambient water, most typically, internal energy, density, and partial pair-correlation functions.

Recent developments of models followed two directions. Some researchers exploiting the increased computer power reparametrized these rigid models like the TIP4P-EW[5] or the TIP4P/2005.[6] The other approach was to develop polarizable models to enhance the range of state variables where the estimates of the model are reasonable. Such models are the GCPM,[7] variants of the COS,[8–10] and the SWM4[11,12] models. While polarizable models are more adequate when the density of water is close to the gas state, in condensed phases their performance is far from satisfactory. In fact, their reparametrized nonpolarizable counterparts predict many properties of water with greater accuracy.[13–15]

In this paper we introduce a new model and demonstrate that it is one of the most powerful classical polarizable models in the literature. The powerfulness of the model comes from the fact that it describes water in the entire state diagram with reasonable accuracy. We believe that this transferable character of the water model is important. If a model has only limited applicability, answers to questions about properties or state variables not used in the fit are less reliable than answers given by a transferable model.

We describe our force field in a systematic fashion explaining our choices. We start with the major features of the model in Sec. II. We discuss options in detail for the geometry (Sec. II A), the charge distribution (Sec. II B), the non-electrostatic interactions (Sec. II C), and the polarizability (Sec. II D). In Sec. III we describe the two major ingredients of the numerical work: handling of long-range forces for Gaussian charge-on-spring particles (Sec. III A) and the integration algorithm for isotherm-isobar systems (Sec. III B). In Sec. IV we parameterize the free variables of the model following a hierarchy of properties in terms of their importance. In Sec. V we present the results. The results are compared with the estimates given by the TIP4P/2005,[6] the GCP,[7] and our recent BKd3[13] models. The first model is a nonpolarizable one but resulted from extensive studies involving the estimation of the entire phase-diagram for water,[16,17] it gives an excellent description in the liquid-solid region. The GCP model,[7] not surprisingly, gives excellent estimates close to the gas phase,[18–20] since this model was deliberately devised for the critical region. TIP4P/2005, a nonpolarizable model, does not work consistently close to the gas phase despite its good estimate of the critical temperature.[15] However, together with the GCP model as a complementary, they cover the phase diagram of water reasonably well. The BKd3 model is a good charge-on-spring polarizable model exploiting the possibility of varying molecular size.[13] This model gives acceptable estimates for properties all over the phase diagram.[14,15] Obviously, there are numerous other models in the literature which might deserve attention, but to review them would widen the scope of this paper too much. Therefore, apart from historically important examples, we restrict ourselves to models related to ours.

First, we discuss the properties calculated for ambient water (Sec. V A). Since we intend to use our model as a solvent, the accuracy of this region has primary importance. In

 

Subsection V B we present properties in terms of the temperature. The anomalous behavior of water is most apparent from its temperature dependence. The description of the vapor-liquid equilibrium with the equilibrium vapor pressure and the surface tension in terms of the temperature is discussed in Subsection V C. Closely related to this, the results of mechanically equilibrated clusters of water up to 6 molecules (Sec. V D) and the temperature dependence of the second virial coefficient (Sec. V E) are presented. The melting properties are discussed in Subsection V F. Finally, we present results of simulations for high-pressure crystalline polymorphs of water (Sec. V G). In Sec. VI we conclude our study.

## II. THE MODEL

### A. Geometry

The geometry of the water molecule is experimentally known in the gas phase. The bond angle is 104.52° and the OH bondlength is 0.9572 Å.[21] These values are used in most models. A notable exception is the SPC[22] model which uses the perfect tetrahedral angle, 109.47°, and 1.0 Å for the bondlengths. We experienced that the role of the bond angle is less important than the bondlength. However, if the dipole moment of the molecule is fixed, the difference in the fitted charges compensates small differences in the geometry. It is known that the OH bondlength is larger than 0.9572 Å in condensed phases.[23] High precision quantum chemical calculations show that although the minimum of the potential energy surface is at 0.9579 Å, the expectation value is 0.9757 Å in the ground state because of the anharmonicity.[24] Therefore, we broke with the tradition and opted for a reasonable value of 0.9750 Å as the OH bondlength. While this value has some arbitrariness, it must be close to the range of actual values in condensed phases.

An important question concerns the vibrations of water which have an inherently quantum mechanical character. There have been attempts in the literature to handle these motions classically. Most notable are the central force methods[25–27] or to equip the classical model with stretching and bending.[1,28,29] Recently, the successful TIP4P/2005 model[6] was also supplemented by classical vibrational modes.[29] The results were similar or only slightly better than that of TIP4P/2005 but the equilibrium OH bondlength had to be chosen unrealistically low: 0.9419 Å. Tironi *et al.* also concluded that the introduction of the flexibility with classical vibrations does not improve the quality of the models significantly,[30] but creates some theoretical and technical problems (e.g., quantum nature of vibrations, shorter timestep). Certainly, there is a possibility to attach vibrations with quantum mechanical nature using the path integral approach.[31–33] The quantum mechanical treatment of the molecule could contribute a lot to understand certain anomalies of water where quantum effects can be significant. Still, these computations are expensive and their overall superiority has not been demonstrated to render powerful classical models obsolete.

So, our choice is a rigid geometry with 104.52° bond angle and 0.9750 Å OH bondlength, and intramolecular vibrations are not included. Using a rigid model we ignore the possibility that the average OH bondlength varies a bit as a function of polarization. It is certainly shorter in the gas phase than in the liquid, and shorter in the liquid than in the ice phases. The rigid model cannot handle this variation which has an impact on the relative stability of liquid water and ice, and will have some effect on intermolecular distances of clusters.

### B. Charge distribution

At first it seems natural to put partial charges on the oxygen and the hydrogen atoms. This arrangement is adopted in the case of the SPC,[22] SPC/E,[3] and TIP3P[4] models. Studies carried out by us showed that this arrangement creates geometries in gas phase clusters not found in experiments or quantum chemical calculations.[34] For these models both the trimers and the tetramers form a completely planar arrangement (all atoms are in the same plane) contrary to the experiment[35] and quantum chemical calculations.[36] We observed that structures close to planar for trimers are more frequent in the liquid phase with SPC-type models than with TIP4P-type ones.[37] This questions the correctness of the many body structure described by SPC-type models. In fact, for three charges a reasonable approximation of the gas-phase quadrupole moments also requires pulling the negative charge closer to the hydrogen atoms.

To picture water where the oxygen atom is in the center of a tetrahedron and the OH bonds and the two nonbonding pairs point towards the vertices seems to agree with chemical theory. One of the first models of water, termed as ST2,[38] used this geometry and so did many following models.[1] The most notable is the recently developed TIP5P force field.[39,40] Our study for clusters showed, however, that the tetrahedral charge distribution creates many low energy clusters with peculiar geometries not found by quantum chemical calculations.[34] And for these tetragonal models the density of the ice Ih crystal is as high as 0.97–0.98 g/cm$^3$, while the experimental value is 0.917 g/cm$^3$.[17]

Vega and co-workers studied the complete phase diagram of nonpolarizable water models.[16,17] They found that the phase diagram is qualitatively incorrect for the SPC and TIP5P-type models (e.g., some ice phases are missing or the hexagonal ice is stable only at negative pressures), but for the TIP4P-type models the phase diagram is qualitatively correct. Therefore, we choose a TIP4P-type charge distribution for our model.

Fifteen years ago Chialvo and Cummings introduced Gaussian charge distributions instead of point charges.[41] Later on, the same idea was utilized in the GCP model.[7] If point charges are converted to Gaussian ones, the multipole moments do not change. The interaction energies and forces of Gaussians are analytical functions. The demand for calculations is larger than that for point charges but the reward is a more realistic description of the electrostatic potential around the molecule and a substantially larger numerical stability. The Gaussian charges are represented by a spherical charge

distribution as follows:

$$\rho_{ia}(\mathbf{r}) = \frac{q_{ia}}{\left(2\pi\sigma_{ia}^2\right)^{3/2}} \exp\left(\frac{-|\mathbf{r}-\mathbf{r}_{ia}|^2}{2\sigma_{ia}^2}\right), \quad (1)$$

where $\rho_{ia}$ is the charge density of site $a$ on molecule $i$, centered at $\mathbf{r}_{ia}$, whose charge is $q_{ia}$ and its distribution width is $\sigma_{ia}$. The corresponding Coulomb interaction energy, $U_{qq}$, between Gaussian charges then becomes

$$U_{qq} = \frac{1}{2}\sum_{i,j\neq i}^{N}\sum_{a,b}\frac{q_{ia}q_{jb}}{4\pi\varepsilon_0\left|\mathbf{r}_{ia}-\mathbf{r}_{jb}\right|} erf\left(\frac{\left|\mathbf{r}_{ia}-\mathbf{r}_{jb}\right|}{\sqrt{2(\sigma_{ia}^2+\sigma_{jb}^2)}}\right), \quad (2)$$

where *erf* is the error function. It can be seen from Eq. (2) that as the distribution width approaches zero, i.e., $\sigma \to 0$, we recover the usual formula for the Coulomb interaction between point charges. The energy is a function of the $\sigma$ − s, the wider the distribution is the higher the energy will be between two opposite charges at the same distance.

The distribution of Gaussian charges can follow the principles established for point charges. The centers of the positive charges are placed on the hydrogen atoms, while the negative charge is positioned on the main axis of the molecule between the hydrogens and the oxygen. In our case the negative charge, −1.168 esu, and its distance from the oxygen, 0.2661 Å, is determined from the requirement that the dipole moment of the molecule matches the experimental gas-phase value, 1.855 D,[42] while the eigenvalues of the quadrupole moment tensor, $Q_{xx} = 2.660$ D Å, $Q_{yy} = -2.335$ D Å, and $Q_{zz} = -0.325$ D Å, were obtained from a least square fit to the experimental values: $Q_{xx} = 2.626$ D Å, $Q_{yy} = -2.493$ D Å, $Q_{zz} = -0.134$ D Å.[43]

### C. Nonelectrostatic interactions

Perhaps, the most canonized interaction in the computer simulation community is the Lennard-Jones function. Two clearly interpreted parameters, simple form, and computational advantages caused its widespread use not only as a model in itself but as an indispensable part of more complicated force fields. Most of the existing water models stuck to this form. While the $r^{-6}$ term correctly describes the distance dependence of the induced dipole-induced dipole interaction, there is no such theoretical justification for the $r^{-12}$ term. Replacing the $r^{-12}$ term with a simple exponential in the form of $A\exp(-Br)$ we could obtain better fits. The $r^{-12}$ repulsion overemphasizes the structure and using a parameter set fitted to ambient liquid provides very poor results for clusters and the second virial coefficient. In addition to this, the exponential function is more realistic describing the repulsion between adjacent molecules as a result of the overlapping electron clouds because the decay of the electron density is exponential at high distances. *Therefore, we use the following form for the nonelectrostatic interactions*:

$$U_{ne} = \sum_{i,j>i}^{N}\left[A\exp\left(-Br_{ij}\right) - C/r_{ij}^6\right], \quad (3)$$

where $r_{ij}$ is the distance between the oxygens of molecule $i$ and $j$.

The exponential form used also by the GCP model[7] is not new. For water it was applied by Errington and Panagiotopoulos[44] in 1998. The potential models of Williams and co-workers[45,46] and the models of alkali-halide crystals or melts[47,48] used exponential repulsions much earlier. The reason that the $r^{-12}$ form is more widespread than exponential repulsion is that the former is computationally much cheaper which was an important factor several decades ago.

### D. Polarization

An inherent weakness of nonpolarizable models is their inability to respond to drastic changes in the environment, most notably, as solvents of biopolymers or in very dilute systems. The need for polarizable models is old[49–52] but usable models appeared only in the late 1980s.[53–55] A more systematic search for polarizable models continued and new models emerged.[56–59]

The experimental gas phase dipole moment of water is 1.855 D.[42] The dipole moment of the molecule changes substantially when moving from the gas state to the condensed state. The polarizability of the gas-phase molecule is close to isotropic, the values of its components are[60] $\alpha_{xx} = 1.4146$ Å$^3$, $\alpha_{yy} = 1.5284$ Å$^3$, and $\alpha_{zz} = 1.4679$ Å$^3$. Since we do not know how these gas-phase values will vary under the influence of finite electric field, the simulation community uses a spherically averaged value of 1.440–1.444 Å$^3$. It turned out studying gas-phase clusters[34] that the isotropic polarizability is essential. The TIP4P-FQ model[56] allows to polarization of the molecule only in the HOH plane. Contrary to experimental and quantum chemical evidences, the trimers and tetramers with this force field are planar just like in the case of the nonpolarizable SPC/E or TIP3P counterparts mentioned above.[34] Among the recent polarizable force fields we did not study the PPC model[58] but its planar polarizability certainly causes the same problem for gas clusters.

There are two methods in the literature to represent isotropic polarization: the polarizable point dipole and the charge-on-spring method. *We opted for the charge-on-spring method for two reasons. First, point dipoles seem less realistic when the intermolecular distances are small. Second and more importantly, handling of the long-range interactions when explicit dipoles are involved is quite cumbersome.*

The idea of charge-on-spring models is the following.[54] A partial charge is connected by a harmonic spring to a predetermined point on the rigid molecular frame. Under an external electric field the spring elongates until the electrostatic and the spring forces cancel each other. This displacement of the partial charge causes the change of the dipole moment. The induced dipole, $\mathbf{p}$ is: $\mathbf{p} = \alpha\mathbf{E} = q\mathbf{l}$, where $q$ is the charge, $\mathbf{l}$ is the elongation vector of the spring, $\alpha$ is the polarizability, and $\mathbf{E}$ is the electric field. From the equality of the electrostatic ($\mathbf{F}_e$) and spring forces ($\mathbf{F}_s$) one has: $q\mathbf{E} = \mathbf{F}_e = -\mathbf{F}_s = k_s\mathbf{l} = k_s\alpha\mathbf{E}/q$. So the spring constant is $k_s = q^2/\alpha$.

This method was used in the SWM4 models[11,12] of water in the form of a Drude oscillator. A partial charge is connected

by a harmonic spring to the oxygen, while another charge with the same size but opposite sign is placed on the oxygen. In the absence of an external polarizing force the spring charge also rests on the oxygen, so the net charge on this atom is zero. The model contains five charged sites. The three remaining point charges, on the hydrogens and on the bisector of the HOH angle, approximate the gas-phase quadrupole moment of the molecule. This model has been parametrized twice. First, the spring charge was chosen to be positive and the charge on the oxygen negative, SWM4-DP,[11] then with a slight refinement of other parameters the spring charge was set to be negative and the oxygen site positive, SWM4-NDP.[12]

Another family of recently published charge-on-spring models is the COS models of van Gunsteren and coworkers.[8–10] In these models, the TIP4P or SPC charge distribution is used but a charge-on-spring particle is connected to the site of the negative charge, therefore, these models contain only four point charges. The first versions, the COS/B[8] models, are based on the SPC model. However, these are not "real" polarizable models because their permanent dipole moment is higher, and the polarizability is lower than the experimental value. The COS/G2 and COS/G3[9] use TIP4P-type charge distribution, the permanent dipole matches the experimental gas-phase value, so they are more consistent models than the COS/B series, and observables computed with them are also much better. In the COS/D[10] model a field-dependent polarizability was introduced to correct the somewhat high dielectric constant of the COS/G models, but the reported expression for the polarization self energy term is erroneous, so the results of this model are not significant.

Recently, we developed a model which was also a charge-on-spring model but it used Gaussian charges.[61] The greater numerical stability against polarization catastrophe without any damping made it possible to use only *three charged sites*: a negative charge served as the charge-on-spring particle and the positive charges rested on the hydrogens. There were three variants of this model. The BKd1[62] has exponential repulsion and constant polarizability (1.444 Å$^3$), and it was fitted not just to ambient water properties but also to properties of hexagonal ice. Since the dielectric constant of the BKd1 model turned out to be too high, in our next model, BKd2,[63] based on theoretical considerations[64] the polarizability was damped at higher electric fields. In the BKd3[13] model this problem was solved in another way: the parameters of the nonelectrostatic interactions were coupled to the induced dipole moment, so a fictive electric field appeared from the nonelectrostatic forces, which reduced the polarization and created molecules with different repulsions and attractions. This method made it possible to fit the parameters to the density-temperature function, which had a positive impact on the melting and critical properties (we will discuss it later in detail).[13–15]

Studying the behavior of our BKd1, BKd2, and BKd3 models we experienced that for models with only one spring charge (or polarizable point dipole) polarization happens most of time along the main axis of the molecule because of the nearly tetrahedral structure of water which creates electric field mainly in this direction. Therefore, these polarizable models were very close to a simplified model when the motion of the negative charge is restricted to the main axis of the molecule, and the negative charge fluctuates around its average position. Since these models try to describe the geometry and charge distribution of the single molecule with achievable accuracy as a starting arrangement, and use physical principles for polarization, flexibility of their fitting abilities is much more restricted than that of their nonpolarizable counterparts for which the charge distribution and nonelectrostatic forces are arbitrary as long as they give good fits to the most important properties. Thus, the advantages of using polarization are strongly reduced by the limited freedom of parameter fits.

The most economic way to get away from this "direction restricted" polarization is to involve the two other charges in polarization as well. Three polarizable charges ensure that the response of the charge distribution to polarization will be not only an elongation in the direction of the main axis but also a more realistic three-dimensional deformation. *We use the conventional 1.44 Å$^3$ polarizability and distribute it between the charges proportional to their magnitudes, so that half of the polarizability (0.72 Å$^3$) is assigned to the negative charge and a quarter (0.36 Å$^3$) is assigned to the positive charges.* One might argue that most of the polarization happens on the oxygen, so the usage of all three charges with the same role is unphysical. However, the model does not mimic the rearrangement of the electron cloud. The charges are used to describe the electrostatic potential around the molecule. During polarization, because of the higher electron density, significant change in the electron structure happens around the oxygen, but this does not mean that the electrostatic potential cannot be described by charges not positioned on the oxygen or very close to it.

The so-called polarization self energy term, which is the work what we have to invest to make induced dipoles, is

$$U_{self} = \frac{1}{2}\sum_i \sum_a \alpha_{ia}\mathbf{E}_{ia}^2 = \frac{1}{2}\sum_i \sum_a \frac{\mathbf{p}_{ia}^2}{\alpha_{ia}}, \qquad (4)$$

where $a$ runs over the charged sites. In charge-on-spring models this energy is none other than the energy stored in the springs.

Our model uses Gaussian charge distributions and exponential repulsion like the GCPM.[7] However, we use charge-on-spring method for polarization with only 3 interacting charges instead of 3 fixed ones and a polarizable point dipole. All 3 charges take part in the polarization.

The schematic diagram of the model is shown in Figure 1.

## III. SIMULATION DETAILS

### A. Handling of the charge-charge interactions

When a model system contains charges special techniques are needed to handle the long-range character of the electrostatic interactions. In the literature there are two methods for this purpose: the Ewald summation and the reaction field method.[65] In this paper we refer to results obtained by the Ewald summation technique. This method has a Hamiltonian which ensures energy conservation. A proper choice

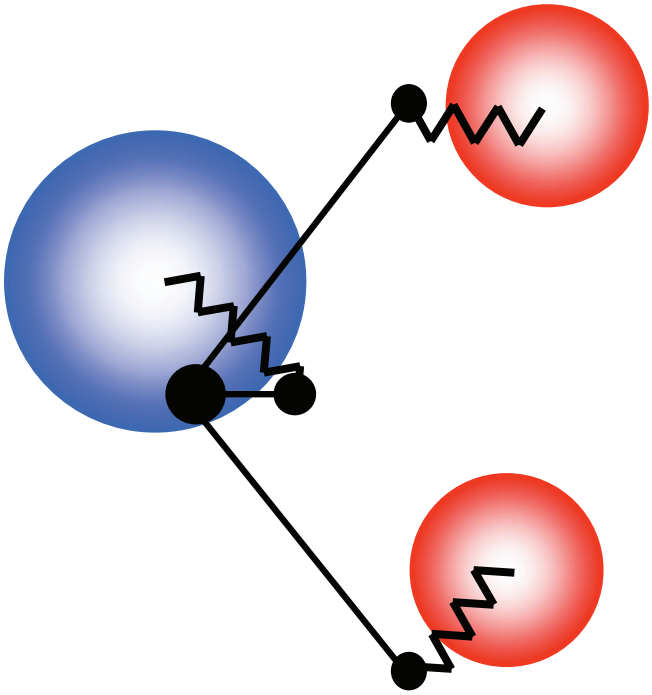

FIG. 1. Schematic depiction of the BK3 model.

of the screening parameter performs this numerically. The reaction field method is a time-saving way to model molecular system by involving continuum electrostatics without rigorous energy conservation.

In our case because we have Gaussian charges the point-charge expressions of Ewald summation are generalized. We provided expressions for the internal energy, forces, and pressure in our previous paper.[61] Since in our model the charge-on-spring particles have no mass, they follow the motion of the nuclei instantaneously. An iterative scheme is needed which does this iteration efficiently in each timestep of the integrating algorithm. We use direct iteration with a predictor scheme to speed up this process. In our previous paper we provided a detailed account about the time-saving methods the program uses including the iteration.[14] We evaluated this scheme for different numbers of iteration and different orders of prediction and found that for a 3rd order prediction 3 iterations are sufficient to obtain a $\cong 2 \times 10^{-5}$ D average error in the induced dipole.[14] This accuracy is mandatory to obtain an accurate internal energy and pressure. There was a widespread view in the simulation community following the paper of Louwerse and Baerends[66] that for polarizable systems modeled under periodic boundary conditions the usual way to calculate the pressure is erroneous. We presented exact derivations and vivid numerical results that the expression for the pressure for charge-on-spring (or polarizable point dipole) polarization is identical with the expression for the nonpolarizable case provided that the mechanical equilibrium between the spring force and the electrostatic force is perfect for each polarizable charge.[67]

The total potential energy of the system in terms of Ewald decomposition consists of the direct and the reciprocal coulombic terms, the nonelectrostatic term, and the polarization self-energy:

$$U_{tot} = U_{dir} + U_{rec} + U_{ne} + U_{self}. \quad (5)$$

It is important to note that since the seminal paper of Berendsen *et al.*[3] the polarization self-energy is considered to be a part of the energy balance of each "ambitious" model. However, in the case of nonpolarizable models this is simply an additive term to the energy which is constant irrespective of the state and surroundings of the molecule, while in the case of polarizable models it is a dynamically changing property of each molecule.

### B. Integration of the equations of motion

The bulk properties calculated with the BK3 model were obtained with a code applying the quaternion formalism[65] but any other bond fixing method could have been applied. The integration for the center of mass motion was done by the isotherm-isobar velocity-Verlet algorithm of Martina *et al.*[68] The rotational degrees of freedom were integrated by the iterative method of Rozmanov and Kusalik.[69] The timestep was 2 fs and typical run-lengths depending on the property to be studied were 2–10 ns. In condensed phases we used 432 particles with the exception of the vapor-liquid coexistence calculations where the system consisted of 1000 particles.

## IV. PARAMETRIZATION OF THE MODEL

The properties of water are very well known from experiments.[2] There are only two features we do not know: the distribution of electric moments in condensed phases and, in the absence of experimental access, the hypothetical low critical point.[2] In this sense the number of properties to match is practically infinite. There is no single parameter set which could fit every property perfectly. Typically, most models establish a hierarchy of properties to fit. For nonpolarizable models these are the density, the internal energy, and the pair-correlation function of for pure water at ambient conditions, possibly the self-diffusion coefficient. Since we intend to mimic many more properties, we should go further in this process. In addition to the density of ambient water, we want an accurate dielectric constant, to describe the temperature-density diagram and to have an accurate density for hexagonal ice. The opposite ends of the phase diagram were not targeted directly because they involve long runs and separate codes. Still, our compromise was to be as good as possible in ambient liquid (density, internal energy, dielectric constant, viscosity, and self-diffusion coefficient) and have the same magnitude of errors at the two ends of the phase diagram.

We found that if the sum of the positive and negative $\sigma - s$ is ~1.06–1.1 Å, the characteristic angle of the dimer (the angle between the O–O line and the main axis of the acceptor molecule) will be very close to the experimental value of 57° which is also advantageous for the structure of condensed phases. While keeping this sum close to this value, we chose $\sigma$-pairs, and targeted ~2.62–2.64 D as the average molecular dipole moment in the liquid because for this model this value ensures the correct dielectric constant. To match other properties, we modified the terms of the repulsive and

TABLE I. Parameters of the BK3 model (see text for details.)

| Geometry | Electrostatics | Polarization | Nonelectrostatic |
|---|---|---|---|
| $d_{OH} = 0.975$ Å | $q_H = 0.584$ esu | $\alpha = 1.44$ Å$^3$ | $A = 322\,000$ kJ mol$^{-1}$ |
| $\theta_{HOH} = 104.52^\circ$ | $q_S = -1.168$ esu | $\alpha_H = 0.25\alpha = 0.36$ Å$^3$ | $B = 3.56$ Å$^{-1}$ |
| $d_{OM} = 0.2661$ Å | $\sigma_H = 0.40$ Å$^{-1}$ | $\alpha_S = 0.5\alpha = 0.72$ Å$^3$ | $C = 3320$ kJ Å$^6$ mol$^{-1}$ |
| | $\sigma_S = 0.71$ Å$^{-1}$ | | |

dispersion forces but maintained the minimum energy of the dimer close to the target value which ensures good estimates for the second virial coefficient. The temperature-density curve was calculated for candidates fulfilling the previous criteria. We experienced from our previous studies that the correct $\rho$–$T$ diagram strongly influences the freezing temperature and determines the critical temperature. *So, we directly fitted the density of ambient liquid and hexagonal ice, the dielectric constant, and the minimum energy of the dimer. The rest of the properties served as an assessment of the fit.* The final parameter set found by this procedure is given in Table I. Obviously, this set is not unique in a sense that choosing a different hierarchy will lead to a different parameter set.

## V. EVALUATION OF THE RESULTS

A model is good if it is simple, based on plausible physical principles and the code does not require too much computer time when averages are collected during long runs. Our code in its present form is a bit more than 4 times slower than the one for a rigid nonpolarizable three-point charge model (e.g., TIP4P) without special speeding-up methods (e.g., particle mesh Ewald). As expected, the same ratio remains if the same speeding-up techniques are applied for both types of models.

However, the models ability to predict properties is the most important criterion. In the following we give an account about this ability for our model that we shall call BK3 and show that its strength is to give good estimates over a long range of the phase diagram. We compare our model with the TIP4P/2005,[6] the GCP,[7] and the BKd3[13] models. At present the TIP4P/2005 has been called the best condensed-phase model of water (with the exception of its dielectric constant),[17] but due to its nonpolarizable character the properties connected to the gas phase are inaccurate or, at least, inconsistent.[15] The GCP is a polarizable model directly fitted to critical properties, therefore, this is the best model for liquid-vapor equilibrium and properties connected to the gas phase.[7,15,18–20] The BKd3 is a charge-on-spring type model which uses only one moving charge to handle the polarization.[13]

Some of the properties can be obtained on the run from the basic code for the bulk phase. The results are long time averages of phase variables collected during the run. However, there are properties which need special variations of the code or entirely new method of calculation. We have already developed all the methodology of calculations when tested our earlier models or models of other authors.[13–15] We provided a detailed account about the possible options to determine one or other properties in these publications. We are not going to repeat these discussions in the present paper but refer the reader to our earlier papers.[13–15] However, for the sake of completeness, we shortly describe some of the methods used for these calculations.

### A. Water at ambient conditions

This is the most studied state of water. Almost every model is fitted to the internal energy, density, and pair-correlation functions of ambient water. In Table II properties of ambient water are shown and compared with the ones of other models.

Diffusion coefficients were calculated using the Einstein equation for the center of mass,

$$D = \lim_{t\to\infty} \frac{1}{6t} \left\langle \frac{1}{N} \sum_{i=1}^{N} [\mathbf{r}_i(t) - \mathbf{r}_i(0)]^2 \right\rangle. \tag{6}$$

Yeh and Hummer[70] showed that the self-diffusion coefficients calculated under periodic boundary conditions depend strongly on the size of the system, and derived a correction factor to eliminate the finite-size effects,

$$D_0 = D_{PBC} + 2.837297 \frac{k_B T}{6\pi \eta L}, \tag{7}$$

where $D_0$ is the self-diffusion coefficients of the infinite system, $D_{PBC}$ is the value calculated under periodic boundaries, $\eta$ is the viscosity, and $L$ is the length of the cubic simulation box. Since its derivation, Eq. (7) has been applied many times.[71–75] Previous studies[70,73] demonstrated that the corrected diffusion coefficients are equal to the extrapolated value for any system size. In Figure 2 the system size dependence of the diffusion coefficient is shown for our simulation.

The shear viscosity was determined by simulations in canonic ($NVT$) ensemble using the Green-Kubo relation,

$$\eta = \frac{V}{k_B T} \int_0^\infty \left\langle \delta P_{\alpha\beta}(t)\, \delta P_{\alpha\beta}(0) \right\rangle dt, \tag{8}$$

where $\delta P_{\alpha\beta}$ is the deviation of the off-diagonal element of the pressure tensor from its average value. Exploiting the symmetry of the system off-diagonal components and the differences between the diagonal components (e.g., $\delta P_{xx}$-$\delta P_{yy}$) are also used in Eq. (8).

The heat capacity, compressibility, and thermal expansivity came from the fluctuations of the corresponding properties,

$$C_p = \frac{\langle H^2 \rangle - \langle H \rangle^2}{N k_B T}, \tag{9}$$

TABLE II. Properties of ambient water (298 K, 1 bar): internal energy $U$, density $\rho$, self-diffusion coefficient $D$, shear viscosity $\eta$, heat capacity $C_p$, compressibility $\kappa_T$, thermal expansion coefficient $\alpha_p$, dielectric constant $\varepsilon$, and average dipole moment $\langle\mu\rangle$. The temperature of maximum density ($T_{md}$) is also shown. The results of the BK3 model were calculated in this work, the numbers in parentheses are the estimated errors in the last digit. Data for the TIP4P/2005, GCPM, and BKd3 models were taken from Refs. 6, 7, 13, and 74. Experimental data were taken from Ref. 2.

| | Expt. | BK3 | TIP4P/2005 | GCPM | BKd3 |
|---|---|---|---|---|---|
| $U$ (kJ mol$^{-1}$) | −41.5 (−43.5) | −43.32(2) | −47.7 | −44.8 | −43.6 |
| $\rho$ (g cm$^{-3}$) | 0.997 | 0.9974(2) | 0.997 | 1.007 | 0.997 |
| $D$ ($10^{-9}$ m$^2$ s$^{-1}$) | 2.30 | 2.28(4) | 2.06[a]; 2.49 | 2.26[a] | 2.43[a] |
| $\eta$ (mPa s) | 0.896 | 0.951(7) | 0.855; 0.83 | | |
| $C_p$ (J mol$^{-1}$ K$^{-1}$) | 75.3 | 91.9(9) | 88 | 94 | 88 |
| $\kappa_T$ ($10^{-6}$ bar$^{-1}$) | 45.3 | 44.4(7) | 46 | ... | 45 |
| $\alpha_p$ ($10^{-4}$ K$^{-1}$) | 2.56 | 3.01(8) | 2.8 | 4.2 | 2.2 |
| $\varepsilon$ | 78.4 | 79(3) | 58 | 84 | 76 |
| $\langle\mu\rangle$ (D) | ... | 2.644(2) | 2.305 | 2.72 | 2.51 |
| $T_{md}$ (K) | 277 | 275(3) | 278 | 255 | 278 |

[a]Neglect the finite-size effects.

$$\kappa_T = \frac{\langle V^2\rangle - \langle V\rangle^2}{\langle V\rangle k_B T}, \tag{10}$$

$$\alpha_P = \frac{\langle VH\rangle - \langle V\rangle\langle H\rangle}{\langle V\rangle k_B T^2}, \tag{11}$$

where the symbols have their usual meanings.

The dielectric constant is proportional to the fluctuation of the total dipole moment of the simulation cell (**M**),

$$\varepsilon = \varepsilon_\infty + \frac{4\pi}{3\langle V\rangle k_B T}\left(\langle \mathbf{M}^2\rangle - \langle \mathbf{M}\rangle^2\right), \tag{12}$$

where $M$ is the sum of instantaneous molecular dipole moments. For the accurate calculation of the dielectric constant very long runs and large systems are required. We used 432 molecules and after 200 ps equilibration performed 6 ns runs, and repeated this procedure 5 times starting from different starting configurations. In Figure 3(a) the convergence of the dielectric constant is demonstrated. All averages reported in Table II were determined from these long simulations.

The experimental internal energy was calculated from the vaporization enthalpy. Its value is −41.5 kJ/mol,[2] but Guillot and Guissani suggested that classical water potentials should fit to a lower value, −43.5 kJ/mol.[76] Their argument

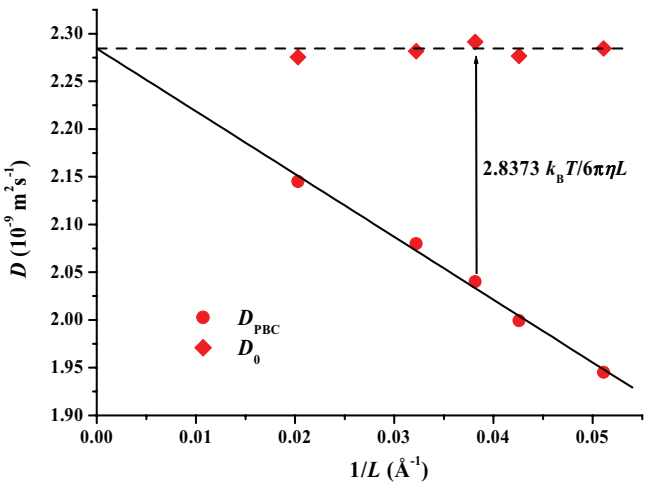


FIG. 2. System size-dependence of the self-diffusion coefficient is shown. The simulated systems contained 250, 432, 600, 1000, and 4000 molecules. The circles and diamonds refer to the uncorrected and corrected values.

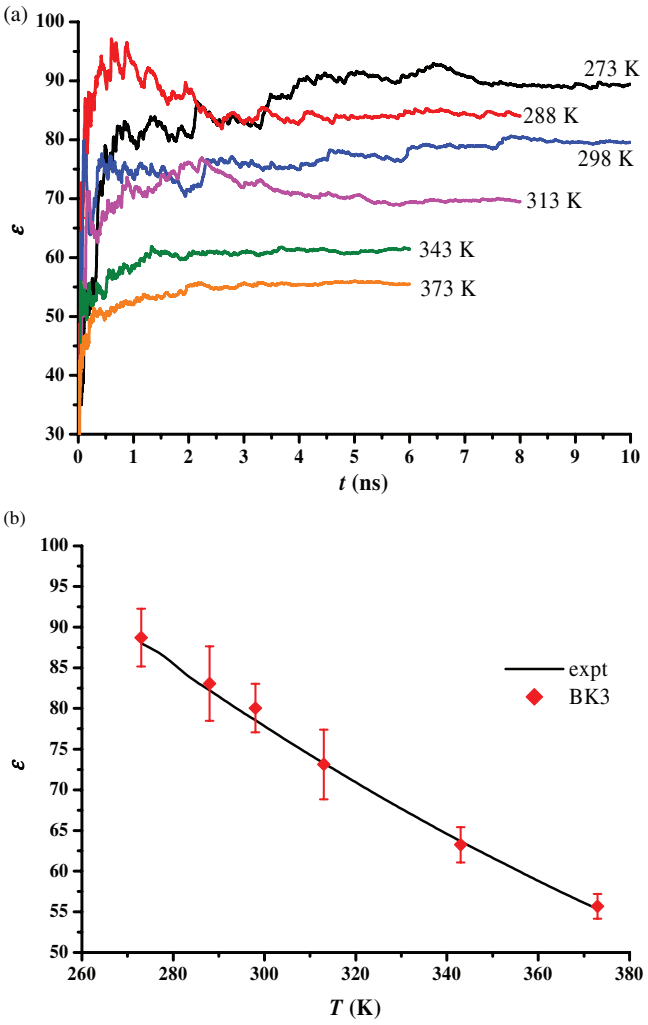


FIG. 3. (a) The convergence of the dielectric constant at different temperatures. (b) The temperature dependence of the dielectric constant of the BK3 model. The error bars were estimated from five runs for each temperature.

is that classical potentials are unable to include quantum effects, yet in the vaporization enthalpy of water the quantum contribution is significant. In the $H_2O$, $D_2O$, $T_2O$ series the quantum effects decrease, therefore, from the extrapolation of the vaporization enthalpies in this sequence one can get the internal energy of the hypothetical "classical" water, which is −43.5 kJ/mol. A similar argument was proposed by Vega *et al.* about to include nuclear quantum effects to obtain a better heat capacity for water.[77] Neglecting nuclear quantum effects the calculated heat capacities will be higher, therefore, it is not worth to fit the internal energy strictly at a given temperature. The experience supports that the internal energy of the most powerful water models, either polarizable or not, should be closer to this lower value (−43.5 kJ/mol) in order to get better agreement for other properties. This is valid for the recent BK3 model, $U$(BK3) = −43.3 kJ/mol, and also for our previous model, $U$(BKd3) = −43.6 kJ/mol. The internal energy of GCPM (−44.8 kJ/mol) is even lower, because this model was devised to obtain good critical properties at the expense of reliable ambient properties. In the TIP4P/2005 model the polarization self-energy term was added to the internal energy. Since this model is nonpolarizable, the polarization self-energy is constant and just shifts the energy scale as mentioned in Sec. III A. Thus, it is our opinion that in simulations with the TIP4P/2005 model the polarization self-energy term should be omitted. Without this term the internal energy of the TIP4P/2005 model is very low, −47.7 kJ/mol.

The density of ambient water was a strict fitting target for every model, so their perfect match is not surprising. The exception is the GCPM, which overestimates the density by 0.007 g/cm$^3$, which is a major shortcoming. The calculated self-diffusion coefficient of the BK3 model includes the finite-size correction discussed above, and it is in good agreement with the experiment. Without finite-size correction the TIP4P/2005 underestimates,[17] with correction overestimates[74] the experimental value. The GCP model did not report using this correction, which means that the relatively good estimate of the model for 256 molecules should be much higher.[7]

Accurate estimation of self-diffusion required the calculation of viscosity which is also an important property of the model on its own. We have no calculated viscosity for the GCP model. The TIP4P/2005 estimate is a bit smaller, while our value is a bit larger than the experimental one.

The heat capacity is too high for all models, which is the consequence of the neglect of nuclear quantum effects.[77] The compressibility of GCPM was not reported, the other models are in good agreement with the experimental value. The agreement for the thermal expansion coefficients is not so good, the estimate of TIP4P/2005 is somewhat better than that for the BK models. The temperature dependence of these properties will be discussed in Sec. V B.

In chemical or biological systems the most important solvent is liquid water. In this respect the dielectric constant is a key property, because it measures the shielding of the Coulomb interactions. Nonpolarizable models often underestimate this property. This is the case for the TIP4P/2005 model. The reported dielectric constant of the GCPM is a preliminary result, it has a large error bar (±15),[7] which makes the reliability of this value questionable. The BK3 model is the best in the estimation of this property.

The primary tool to describe the structure of liquid water is the three partial pair-correlation functions. These functions can be obtained by neutron and (for the OO part) x-ray scattering measurements, however, with limited accuracy. There are important features of these curves, like the place and height of the first OO peak and the first minimum. The partial pair-correlation functions are shown in Figure 4. The first peak of the oxygen-oxygen pair-correlation function is high for the TIP4P/2005 model, because the $r^{-12}$ repulsion creates a more structured liquid. This peak is lower but still high for the BKd3, which has less steep $r^{-10}$ repulsion. With an exponential repulsion (BK3 and GCP models) the height of the first peak is correct. The OO structure of the BK3 is the closest to the experimental, the first minima of the $g_{OO}(r)$ function of the GCPM in not deep enough. The difference in the predicted OH and HH pair-structures of these models is negligible. The first peak of the OH pair-correlation function, which belongs to the hydrogen bonds, is narrower and higher than the experimental ones, because of the fixed bondlength of the models. Otherwise, agreement with the experiment is good, particularly if we consider that the experimental error bar of the measured OH and HH pair-correlation functions is larger than that for the OO function.

### B. Properties in terms of the temperature

The temperature dependence of the density of liquid water is very important. Unfortunately, it is difficult to reproduce with classical potentials.[13] At 1 bar the function has a maximum at 277 K (temperature of maximum density, $T_{md}$). The density-temperature ($\rho$–$T$) diagram correlates strongly with the melting and critical properties. As we showed previously, if the water densities are too high at low temperatures, the melting temperature will be low.[14] If this curve decreases too steeply at high temperatures, the critical temperature will be underestimated.[15] In Figure 5 the $\rho$–$T$ diagrams are shown. The curve for the GCPM matches the experimental one at high temperatures, which is a consequence of fitting to critical properties. However, it is very high at low temperatures. The other three models were fitted to the $\rho$–$T$ curve, therefore, their $T_{md}$s are very close to 277 K. This fitting was most successful for the TIP4P/2005 model. The BKd3 has excellent results at high temperatures, but below 300 K it is significantly worse than the TIP4P/2005 or the BK3. The BK3 result is only slightly worse than that of the TIP4P/2005. At low temperatures it is a bit higher, at high temperatures it is a bit lower than the experimental curve.

As mentioned previously the dielectric constant is a very important property of molecular models of solvents. For the BK3 water model it agrees well with the experimental values not just at ambient conditions, but over a temperature range from 0 °C to 100 °C, as shown in Figure 3(b).

The prediction of the self-diffusion coefficient is the best for the BK3 model at 1 bar in the 270–370 K temperature range (see Figure 6(a)) relative to the other models shown.

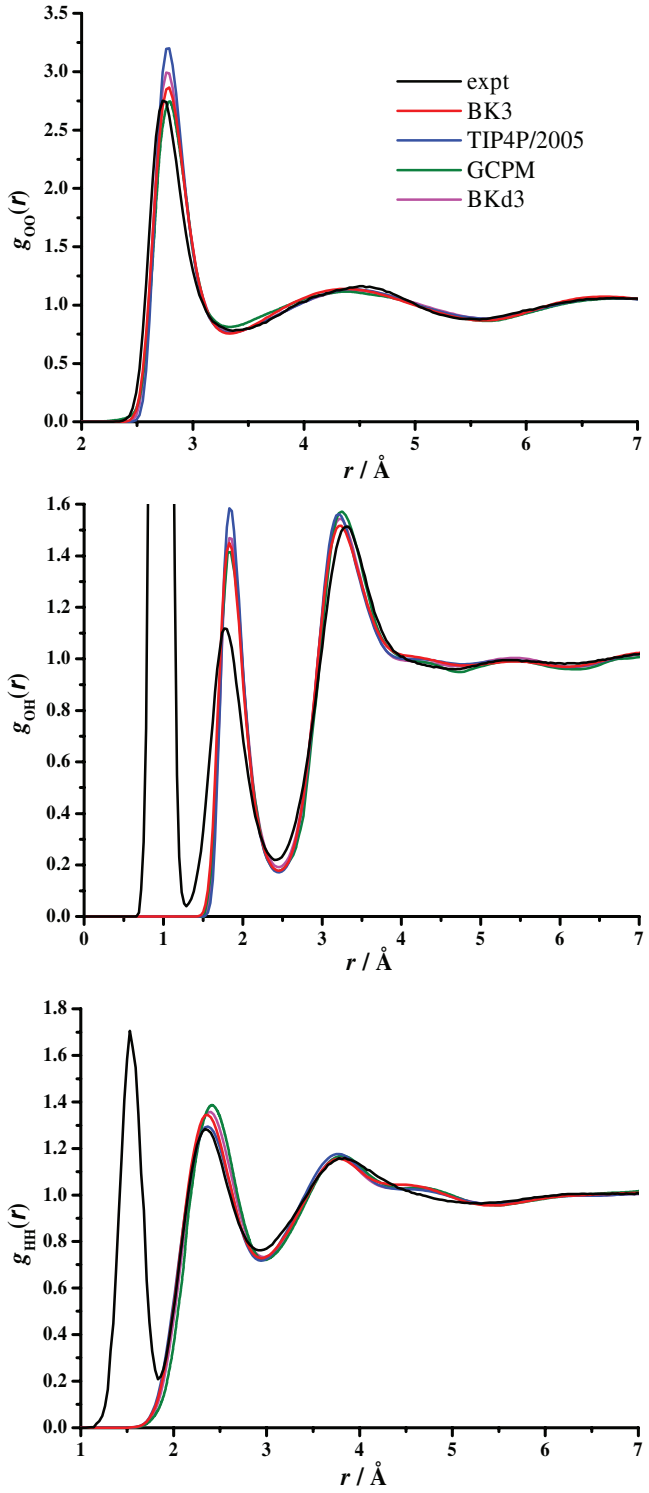


FIG. 4. Oxygen–oxygen (top), oxygen–hydrogen (middle), and hydrogen–hydrogen (bottom) pair-correlation functions at ambient conditions, 298 K and 1 bar. The experimental data are from Ref. 91.

The TIP4P/2005 and GCP model underestimate the diffusion coefficient at higher temperatures if the finite-size correction is not applied. If it were included, it would correct their estimates at high temperatures, but worsen the agreement at low temperatures (see the discussion about the ambient diffusion coefficient in Sec. IV A) Inclusion of the correction for the

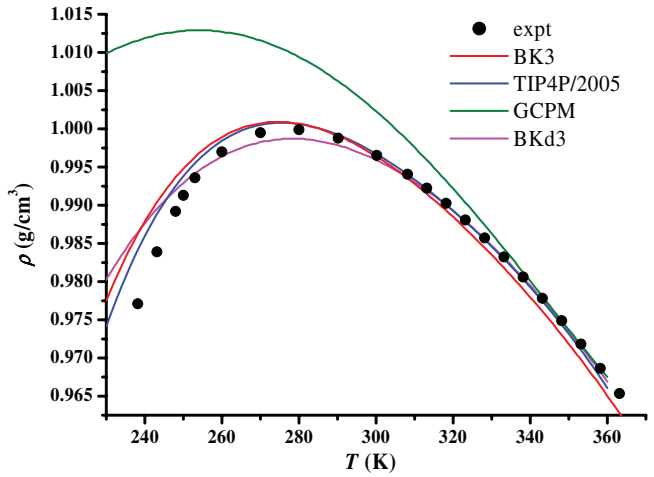


FIG. 5. The density of the liquid water at 1 bar as a function of temperature.

BKd3 model would overestimate the diffusion coefficient at all temperatures.

In Figure 6(b) the temperature dependence of the viscosity is shown for the BK3 model. The agreement is remarkable if one takes into account that this is not a fitted property.

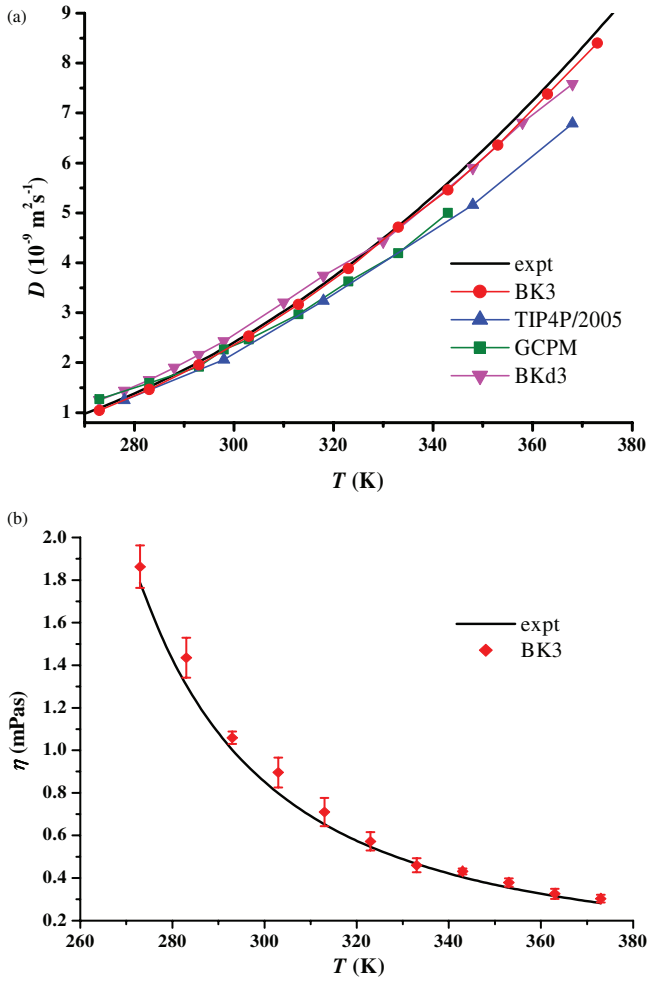


FIG. 6. (a) Self-diffusion coefficients as function of temperature. Finite size corrections are included only for BK3 model. (b) Shear viscosity of the BK3 model as a function of temperature. The error bars were estimated from using different off-diagonal components for the calculation.

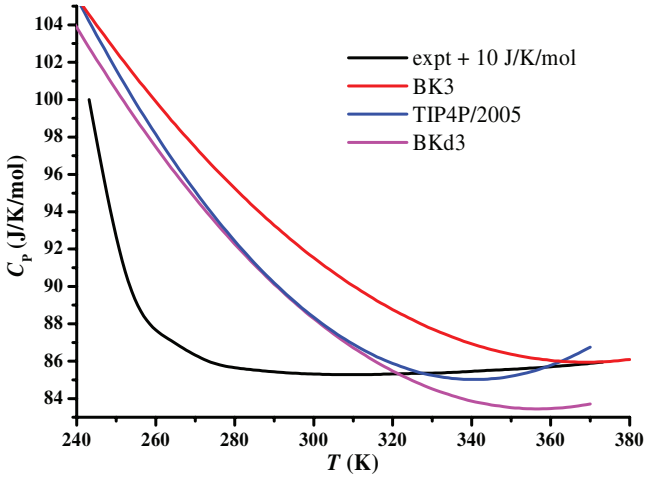


FIG. 7. The temperature dependence of the isobaric heat capacity at 1 bar. The experimental line was shifted up by 10 J $K^{-1}$ $mol^{-1}$ for better comparison.

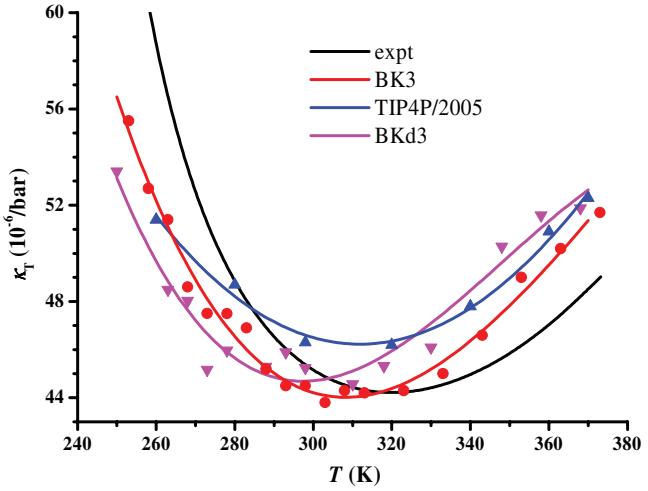


FIG. 9. The temperature dependence of the compressibility at 1 bar. The marks are the simulated values which have relatively large statistical noise. The lines are fitted fourth order polynomials.

The temperature dependence of the fluctuation-related properties is shown in Figures 7–9. We fitted polynomials to the $H(T)$ and $\rho(T)$ functions, and the heat capacity and thermal expansivity were calculated analytically from the derivative of the fitted polynomials. In the heat capacity diagram the experimental curve was shifted up by 10 J/K/mol for better comparison, because all of these models have higher heat capacity than the experimental one. It is because there is no inclusion of nuclear quantum effects.[77] Similar to the density, the heat capacity also shows an extremum as a function of temperature, it has a shallow minimum at 309 K. The heat capacity of the models shown here is qualitatively good in that respect that they also have a minimum, but it is at higher temperatures, about 340 K, 355 K, and 365 K for the TIP4P/2005, BKd3, and BK3 models, respectively. The shape of the curves is also not correct, they decrease too slowly in the supercooled region, therefore, their minima is not as shallow as that of the experimental curve. Although the TIP4P/2005 seems a bit better than the BK3 or BKd3, the deviations from the experimental data are much larger than the differences between the models.

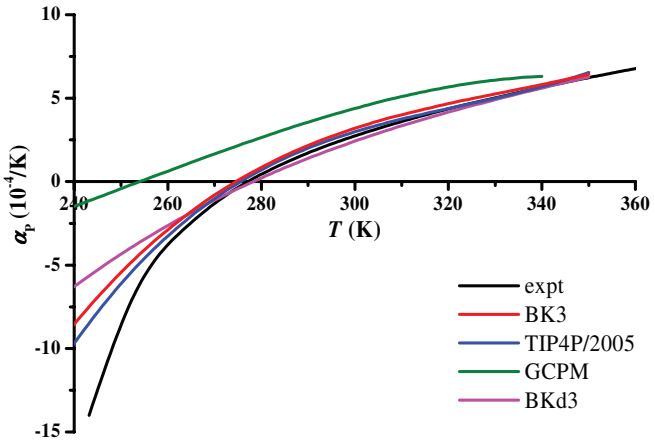


FIG. 8. Thermal expansion coefficient as a function of temperature at 1 bar. The crossing of the curves with the $T$ axis gives the $T_{md}$.

The thermal expansivity function is the derivative of the density-temperature function, therefore, the performance of the models is similar to what we have experienced in the $\rho$–$T$ curves. The GCPM overestimates the thermal expansivity below 340 K and its $T_{md}$ is very low: 255 K. The other models have correct $T_{md}$s. The thermal expansivity of the BKd3 model is somewhat high at lower temperatures. The results of the BK3 model are slightly worse than the results of the TIP4P/2005 but both models are very close to the experimental curve.

Similar to the heat capacity the isothermal compressibility also has a minimum, which is at 320 K. In Figure 9 preliminary results are shown for the BK3 and BKd3 models. The compressibility was calculated from the volume fluctuation (Eq. (10)), therefore, longer simulations are needed to reduce the statistical noise and get smooth curves, but the trends are visible. The BKd3, TIP4P/2005, and BK3 models reproduce the compressibility anomaly quite well, they all have minima, and the estimated values differ from the experimental less than 10%. The BKd3 has the largest difference in terms of the position of the minimum (about 20 K), the BK3 and TIP4P/2005 models are better. Overall, the BK3 model gives the best compressibility-temperature function. The curve of the BK3 compressibility is very similar to the experimental one, with the difference that it is shifted down by 10 K. At low temperatures the compressibility of the TIP4P/2005 model decreases too slowly.

### C. Vapor-liquid equilibrium and critical properties

Critical properties and the vapor phase received much more attention than the solid phase discussed in the next chapter. First, it is motivated by the industrial importance of supercritical technology. Second, the polarization of a water molecule hydrating apolar solutes is similar to that in dilute state at high temperature.

To calculate this property we had to leave the usual homogeneous bulk code and create a two-phase cell. So the

vapor-liquid equilibrium has been determined by direct coexistence *NVT*-MD simulations in a rectangular box containing 1000 molecules. The size of the box was 28.0 Å × 28.0 Å × 120.0 Å and the averages were collected over 2 ns on a well equilibrated sample.

Alejandre *et al.* showed that using this geometry the number of reciprocal vectors has to be increased in the direction perpendicular to the interface.[78] Our values were $|k_x^{\max}| = |k_y^{\max}| = 5$ and $|k_z^{\max}| = 25$.

The equilibrium vapor and liquid densities were determined by fitting a hyperbolic tangent function to the density distributions,

$$\rho(z) = \frac{1}{2}(\rho_l + \rho_v) - \frac{1}{2}(\rho_l - \rho_v)\tanh\left(\frac{z - z_0}{\delta}\right), \quad (13)$$

where $\rho_v$ and $\rho_l$ are the vapor and liquid densities and the $\delta$ parameter is related to the width of the interface. The critical temperature and density were estimated from the density data above 400 K using the law of rectilinear diameters,[79]

$$\frac{\rho_l + \rho_v}{2\rho_c} = 1 + D_0|\tau| \quad (14)$$

and the Wegner expansion[80]

$$\frac{\rho_l - \rho_v}{\rho_c} = A_0|\tau|^{\beta}, \quad (15)$$

where $\tau = 1 - T/T_c$ and $\beta = 0.325$.

The equilibrium vapor pressure in direct coexistence simulations is the normal component of the pressure tensor, $P_v = P_{ZZ}$. To determine the critical pressure we fitted the vapor pressure curve with Antoine's law,

$$\ln P_v = A + \frac{B}{T + C}. \quad (16)$$

The main advantage of the direct coexistence simulations is the existence of the surface, therefore, surface properties, such as the surface tension, can also be calculated,

$$\gamma = \frac{V}{2A}\left\langle P_{ZZ} - \frac{1}{2}(P_{XX} + P_{YY})\right\rangle, \quad (17)$$

where $V$ is the volume of the simulation cell, $A$ is the area of the surface, and $P_{XX}$, $P_{YY}$, and $P_{ZZ}$ are the corresponding elements of the pressure tensor. The 1/2 factor is because of the two interfaces in the simulation box. The usual long range correction of the dispersion forces was taken into account,[81]

$$\gamma_{LRC} = \frac{\pi}{2}(\rho_l - \rho_v)^2 \int_0^1 ds \int_{Rc}^{\infty} dr \coth\left(\frac{rs}{\delta}\right) \times \frac{dU_{ne}}{dr} r^4(3s^3 - s). \quad (18)$$

In Figure 10 the equilibrium vapor and liquid densities are shown, while in Table III the critical properties are summarized. The BK3 model has a slightly lower critical temperature than the other models or the experimental value, and, therefore, the equilibrium vapor and liquid densities are also somewhat lower. The strict correlation between the high temperature part of the $\rho$–$T$ diagram and the critical temperature is observed again. The GCP model is the only one which was explicitly fitted to the critical point, so its excellent result concerning $T_c$ is not surprising. But since the fitting range of this

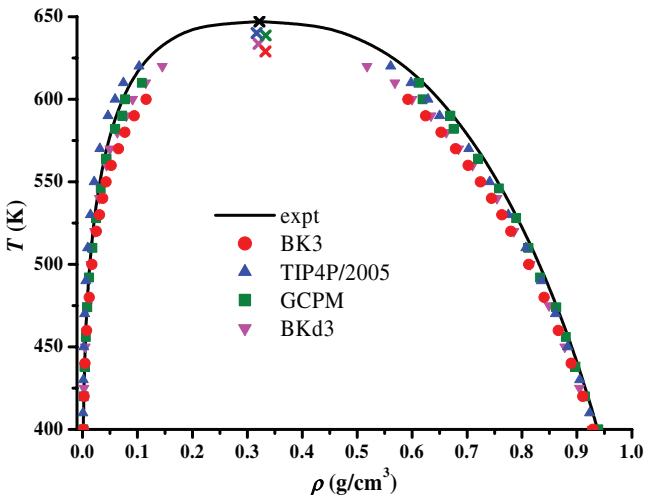


FIG. 10. Vapor-liquid coexistence curves. The crosses indicate the corresponding critical points.

model is limited to this region, the model has deficiencies at lower temperatures, such as the ambient water density, internal energy, and dielectric constant, as shown in Secs. V A and V B. For the BKd3 and TIP4P/2005 models the parameter fit was aimed at a wider range of thermodynamic states.[6,13] Their estimates for the critical temperature are very good because of the correct estimation of the high temperature part of the $\rho$–$T$ curve. The slightly worse performance of the BK3 model can be explained by the compromises during the parameter fit. The two parts of the $\rho$–$T$ diagram were in competition. If we fitted the high-temperature part of the diagram more accurately, the low-temperature part would have worsened and the freezing point would have been lower. Still, $T_c = 629$ K is a reasonable value because most of the polarizable models (SCPDP, DC, COS, and SWM4 family) have critical temperatures well below of 600 K (see Table I in Ref. 15).

In Figure 11 the equilibrium vapor pressure and also the critical pressure is presented. Nonpolarizable models are unable to predict gas phase-related properties accurately, thus, the TIP4P/2005 model has too low vapor and critical pressures. The vapor pressure curves of BKd3 and GCPM are very similar and close to the experimental one. The critical pressure of the BK3 is good, but its vapor pressures are a bit high. This overestimation is the consequence of the lower critical temperature, which can be demonstrated by presenting the vapor pressures as a function of the reduced temperature, $T/T_c$ (see Figure 11(b)). Here, the results of all three polarizable models match the experiment, which means that their

TABLE III. Critical temperature, ($T_c$), pressure, ($P_c$), and density, ($\rho_c$), for different models. The results for the BK3 model were calculated in this work, the results of TIP4P/2005, GCPM, and BKd3 models were taken from Refs. 17, 7, and 13, respectively. Experimental data were taken from Ref. 2.

| | Expt. | BK3 | TIP4P/2005 | GCPM | BKd3 |
|---|---|---|---|---|---|
| $T_c$ (K) | 647 | 629(5) | 640 | 642 | 634 |
| $P_c$ (bar) | 220 | 233(8) | 146 | 246 | 214 |
| $\rho_c$ (g/cm$^3$) | 0.322 | 0.333(11) | 0.310 | 0.334 | 0.320 |

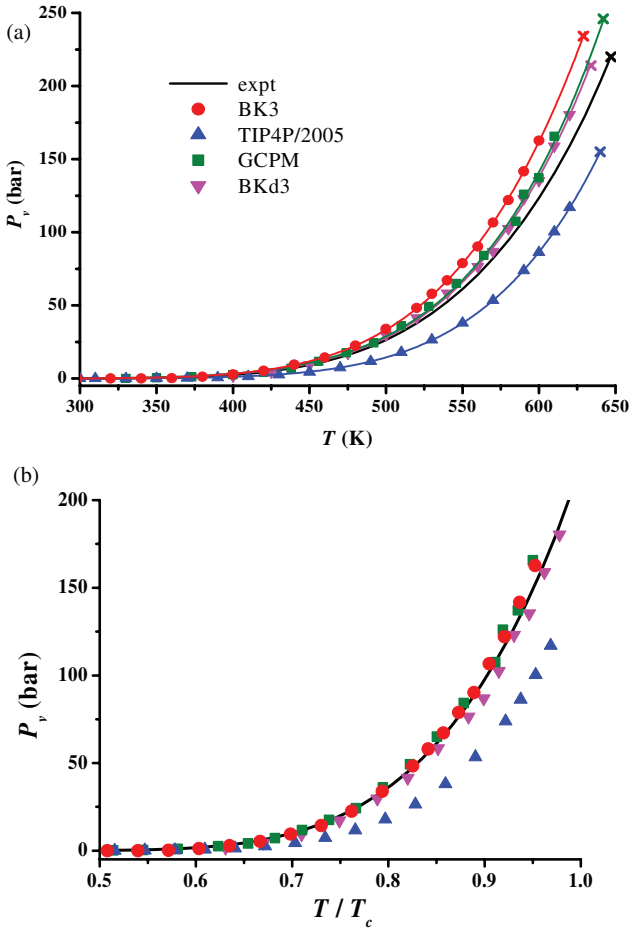


FIG. 11. (a) Equilibrium vapor pressures as a function of temperature. The crosses indicate the critical points. (b) Same as in (a) but using the corresponding reduced temperature ($T/T_c$) as independent variable.

vapor pressures are consistent with the critical temperature. However, this is not true for TIP4P/2005.

The surface tension for ambient water by GCPM is 68.85 mN/m[82] which is close to the experimental 72 mN/m. The surface tension for other models discussed here is given in a wide temperature range (see Figure 12). It should be noted that the usual long range correction for the dispersion forces is not taken into account for BKd3 because the varying molecular size of this model would make the calculation very cumbersome. For the other two models the tail correction given by Eq. (18) was included. Below 400 K the results of the BK3 and TIP4P/2005[83] models are very similar and only slightly lower than the experimental value. The ambient values are 68.2 and 69.2 mN/m for BK3 and TIP4P/2005, respectively. The surface tension goes to zero at the critical point, therefore, it is expected that the model which has a critical temperature closer to the experimental one, has better results for the surface tension. Because of this the surface tension for TIP4P/2005 is better than that for BK3 at higher temperatures. In this respect, compared to other charge-on-spring type polarizable models, the BK3 can be called the best. (See surface tension data for COS and SWM4 models in Ref. 15.)

The vaporization enthalpies as a function of temperature are shown in Figure 13. The experimental curve starts from

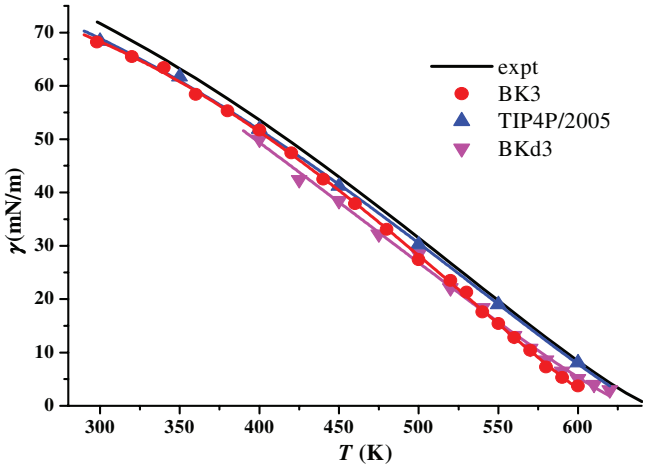


FIG. 12. Surface tension as a function of temperature. With the exception of the BKd3 model the tail correction of the dispersion forced is included.

44.0 kJ/mol at 298 K and goes to zero at the critical point The models have lower internal energy at ambient conditions (as discussed in Sec. IV A), therefore, their vaporization enthalpy is higher at 298 K, the highest is for TIP4P/2005 and the lowest is for BK3. As we showed previously the vaporization enthalpy curves of the water models are steeper than the experimental ones, for models with point charges they are steeper than for models with Gaussian charge distributions.[15] This is also an advantage of using Gaussian charges. Consequently, at lower temperatures (below 500 K) the BK3 model gives the best estimations for the vaporization enthalpy, but since it has a somewhat lower critical point than the other models at high temperatures GCPM and TIP4P/2005 are better.

### D. Gas phase clusters

A few years ago we studied gas clusters of water up to 6 molecules.[34] We identified not only the lowest energy conformations but all arrangements with reasonably low energy. This study pointed out that only water models with TIP4P-type charge distribution give qualitatively correct geometries.

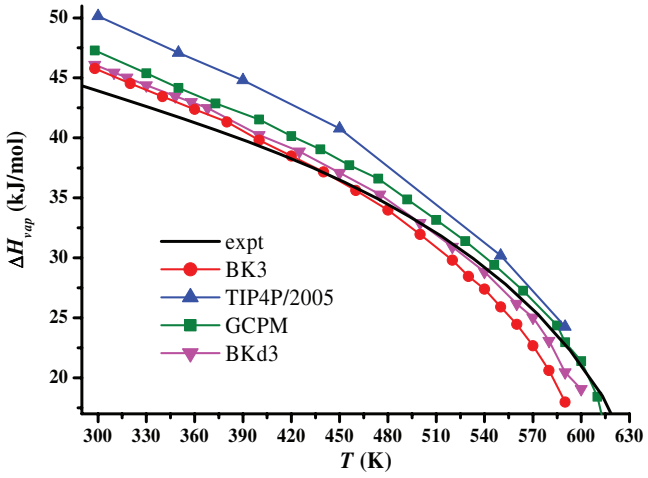


FIG. 13. Vaporization enthalpies as a function of temperature. The marks indicate simulated points and the lines are help for the eye.

TABLE IV. Energies ($E$) and average oxygen–oxygen distances ($d_{OO}$) of small water clusters for different models. The energies are in kJ/mol and the distances are in Å. In the case of the dimer the characteristic angle, $\theta$ (the angle between the OO line and the symmetry axis of the acceptor molecule), and the total dipole moment, ($\mu_{tot}$), are also shown. QC refers to the highest level quantum chemical calculations (Refs. 36 and 84). Experimental data were taken from Refs. 35 and 85.

| | | Expt. | QC | BK3 | TIP4P/2005 | GCPM | BKd3 |
|---|---|---|---|---|---|---|---|
| Dimer | $E$ | $-22.6 \pm 2.9$ | $-20.92$ | $-20.63$ | $-28.71$ | $-20.77$ | $-22.41$ |
| | $d_{OO}$ | 2.94 | 2.91 | 2.874 | 2.770 | 2.877 | 2.815 |
| | $\theta$ | 57 | 58 | 53.6 | 49.0 | 55.3 | 56.6 |
| | $\mu_{tot}$ | 2.60 | 2.6 | 2.648 | 2.885 | 2.617 | 2.031 |
| Trimer | $E$ | | $-66.10$ | $-64.23$ | $-76.99$ | $-60.67$ | $-66.23$ |
| | $d_{OO}$ | 2.96 | 2.80 | 2.805 | 2.784 | 2.838 | 2.782 |
| Tetramer | $E$ | | $-115.6$ | $-109.0$ | $-128.3$ | $-106.4$ | $-112.6$ |
| | $d_{OO}$ | | | 2.761 | 2.745 | 2.773 | 2.743 |
| Pentamer | $E$ | | $-151.8$ | $-143.3$ | $-167.3$ | $-142.9$ | $-148.6$ |
| | $d_{OO}$ | | | 2.748 | 2.743 | 2.749 | 2.731 |
| Prism | $E$ | | $-192.0$ | $-192.4$ | $-216.5$ | $-181.8$ | $-194.7$ |
| | $d_{OO}$ | | | 2.816 | 2.813 | 2.858 | 2.804 |
| Cage | $E$ | | $-191.6$ | $-190.5$ | $-218.0$ | $-181.9$ | $-193.5$ |
| | $d_{OO}$ | | | 2.797 | 2.779 | 2.828 | 2.784 |
| Book | $E$ | | $-190.8$ | $-183.0$ | $-212.4$ | $-180.5$ | $-188.9$ |
| | $d_{OO}$ | | | 2.776 | 2.757 | 2.785 | 2.758 |
| Cyclic | $E$ | | $-187.4$ | $-175.8$ | $-204.2$ | $-177.3$ | $-183.2$ |
| | $d_{OO}$ | | | 2.743 | 2.743 | 2.737 | 2.725 |

If polarization is introduced, then it has to be isotropic, because polarization restricted to the molecular plane (fluctuating charge models) causes erroneous geometries as well.[34] The TIP4P, GCPM, BKd3, and BK3 models fulfilled these criteria, the geometries of their clusters are qualitatively correct. The quantitative results, energies, and oxygen-oxygen distances are summarized in Table IV compared to the highest level quantum chemical calculations[36,84] and, when available, to experimental data.[35,85]

As a result of fitting compromises we could not choose the parameter set to match the properties of the dimer. We had to lower the characteristic angle from ∼57° to 54° and our energy is also slightly higher than the quantum chemical result. The most difficult part is to obtain the experimental 2.94 Å OO distance for dimer even for quantum chemical studies. Our result is considerably smaller but it is important to note that it is 0.1 Å longer than the first peak on the OO pair-correlation function in liquid water. In the case of the TIP4P/2005, similar to other nonpolarizable models, these two values are practically identical (∼2.77 Å), which is mainly the result of the $r^{-12}$ repulsion. Due to the less steep $r^{-10}$ repulsion the dimer energy and OO distance of the BKd3 model are better, but still far from the best quantum chemical values.[84] The results of the BK3 and GCP models again clearly show the advantages of the exponential repulsion.

With the exception of the OO distance in the trimer,[34] there are no experimental data for water clusters formed by several molecules, therefore, quantum chemical calculations were used as references. The minimum energy conformation of the clusters $(H_2O)_n$ $n = 3$–5 is the cyclic form. The hexamer is the first cluster where a spatial rearrangement (prism) is the global minimum. Three other low energy configurations (cage, book, cyclic) are also often studied, and the energy sequence of these configurations is an important trait of classical water potentials.[34] The polarization is essential to get reasonable energies for clusters, the nonpolarizable models, including TIP4P/2005, severely underestimate the energies. In total, the BK3 gives the best results for small water clusters. Although the dimer properties of GCPM are slightly better, the BK3 energies for larger clusters, especially for hexamers, are closer to the QC values.

### E. Second virial coefficient

The temperature dependence of the second virial coefficient is an informative property about the intermolecular potential energy surface, since it depends not only on a particular point (like the dimer energy) but on the whole surface. The second virial coefficient can be calculated from the interaction energy of two molecular configurations,

$$B(T) = -\frac{N_A}{16\pi^2}\int_0^\infty r^2 dr \int_0^\pi \sin\theta d\theta \int_0^{2\pi} d\varphi \int_0^{2\pi} d\omega_1 \times \int_0^\pi \sin\omega_2 d\omega_2 \int_0^\pi d\omega_3 \times \left\{1 - \exp\left[-\frac{U(r,\theta,\varphi,\omega)}{k_B T}\right]\right\}, \quad (19)$$

where $N_A$ is the Avogadro's number, $k_B$ is the Boltzmann constant, $T$ is the temperature, and the $(r, \theta, \varphi)$ polar coordinates and $(\omega_1, \omega_2, \omega_3)$ Euler angles describe the relative orientation of two molecules. While this equation is straightforward, a separate program is needed to carry out the integration. In our program the radial integration was divided into three intervals. For distances below 2.0 Å the hard sphere approximation was used, and over 10.0 Å, when the polarization effect is negligible, the interaction between the two molecules is approximated by dipole-dipole interaction. The analytical solution is

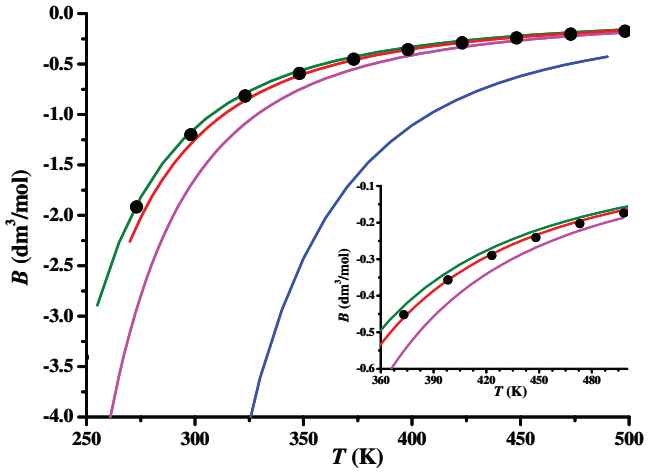


FIG. 14. Temperature dependence of the second virial coefficient. In the inset the high temperature region is enlarged. The meaning of the colors is the same as in other figures: green-GCPM; blue-TIP4P/2005; red- BK3; pink-BKd3.

known for these cases.[86] Between 2.0 Å and 10.0 Å the integral was calculated by Monte Carlo sampling[87] with $\sim 10^8$ randomly chosen configurations.

The results are presented in Figure 14. The nonpolarizable models are not able to describe the gas and condensed phase properties simultaneously. Because of the higher dipole moment, the interaction energies of two molecular configurations are too low for the TIP4P/2005 model. Therefore, the virial coefficient is underestimated by a factor of ~5-6. The polarizable models are better. BKd3 somewhat underestimates the virial, as expected from the lower dimer energy, but GCPM and BK3 give correct results. First, one may think that the GCPM is significantly better than BK3, but the inset in Figure 14 shows that GCPM is more accurate at low temperatures and BK3 is more accurate at high temperatures. Here, it is also important to note that none of our models were fitted explicitly to the second virial coefficient.

### F. Melting properties

Most of water models are not tested in the solid phase. In addition to studying ice for its own interest, this can be important for other reasons as well. The structure of hexagonal ice is stable below 273 K at 1 bar which is not very far from the conditions of water used as a solvent. This means that, at least temporally, ice-like clusters may form during solvation. The melting point of water is one of the most difficult properties to reproduce. The calculation is quite expensive. Detailed discussion of methods is given in our previous paper,[14] and there is a detailed review by Vega and co-workers.[88]

To calculate the melting temperature of the BK3 model we applied the same method what we used previously for the COS, SWM4, and BKd models.[14] The essence of this method is to find the temperature where the Gibbs free energy difference between the liquid and solid phases is zero. The Gibbs free energy can be calculated with thermodynamic integration (TI). To do this we need a reference point. In this work we used the TIP4P/2005 model as a reference. Its melting point at 1 bar is 250 K, which was confirmed by using different methods.[6,89,90] The Gibbs free energy of the coexisting phases for the TIP4P/2005 at the melting point is equal. This was the zero point of our free energy scale. In the first step the free energies of the liquid and solid phase of the BK3 model were calculated relative to this zero point by thermodynamic integration.

Let us define a $\lambda \in [0, 1]$ parameter, which couples continuously the reference TIP4P/2005 system (marked $A$) to the examined BK3 system (marked $B$),

$$U(\lambda) = U_A + \lambda (U_B - U_A). \tag{20}$$

The difference between the Gibbs free energies of systems $B$ and $A$ at temperature $T_0$ is

$$G_B(T_0) - G_A(T_0) = \int_0^1 \left\langle \frac{\partial U(\lambda)}{\partial \lambda} \right\rangle_{N,P,T_0,\lambda} d\lambda = \int_0^1 \langle U_B - U_A \rangle_{N,P,T_0,\lambda} d\lambda, \tag{21}$$

where $\langle \dots \rangle$ denotes an ensemble average and $T_0$ is the melting point of the reference system. The integral was calculated by Gauss-Legendre quadrature with 8 quadrature points. Calculating this value for the solid and for the liquid phase, we got the free energy difference between them for system $B$ at $T_0$. The second step is to calculate the temperature dependence of the free energy difference with the integrated form of the Gibbs-Helmholtz equation,

$$\frac{\Delta G_B(T)}{T} = \frac{\Delta G_B(T_0)}{T_0} - \int_{T0}^{T} \frac{\Delta H_B(T')}{T'^2} dT'. \tag{22}$$

To obtain numbers for the above equation, the $H_B(T)$ functions for water and ice should be determined by a series of $NPT$ simulations in a corresponding temperature range. At the melting point $\Delta G_B$ becomes zero. Note that in this method only relative free energies are used, the zero point of the free energy scale is the free energy of the reference system at its melting point. The advantage of this method is that it is feasible even if the absolute free energy of the reference system is not known. It often occurs, for example, if the melting point was determined by direct coexistence simulations or Gibbs-Duhem integration. To check the consistence of our calculations we repeated this procedure using the TIP4P/Ice ($T_m = 270$ K) model as reference. The obtained melting temperatures were within 0.5 K.

Melting temperatures and other melting properties are summarized in Table V. For GCP model data are not available in the literature, but because of the correlation between the low temperature part of the $\rho$–$T$ function and the melting temperature,[14] we assume that its melting point is low. The melting properties of the BK3 and TIP4P/2005 models are very similar and significantly better than that of the BKd3 model. The melting temperature is 250 K, underestimating the experimental value by 20–25 K. At first glance this deviation may seem high, but considering the results of other models this 250 K value is the best estimate. The models which have higher melting temperature have unacceptably large errors in other properties, e.g., the melting point of the TIP5P model is 273 K, but the density of ice Ih is 0.97-0.98 g/cm$^3$ and

TABLE V. Melting properties of ice Ih at 1 bar for different models. $T_m$ is the melting temperature, $\rho_l$ and $\rho_s$ are the densities of the equilibrium liquid and solid phases, $H_l$ and $H_s$ are the corresponding enthalpies, $\Delta H$ is the melting enthalpy, $\Delta S$ it the melting entropy, and $dp/dT$ is the slope of the ice Ih-water equilibrium line at 1 bar. The results of the BK3 model were calculated in this work, data for the TIP4P/2005 and BKd3 models were taken from Refs. 6 and 14. Experimental data were taken from Ref. 2.

| | Expt. | BK3 | TIP4P/2005 | BKd3 |
|---|---|---|---|---|
| $T_m$ (K) | 273.15 | 250(3) | 250 | 233 |
| $\rho_l$ (g/cm$^3$) | 0.999 | 0.995 | 0.993 | 0.983 |
| $\rho_s$ (g/cm$^3$) | 0.917 | 0.924 | 0.921 | 0.921 |
| $H_l$ (kJ/mol) | | − 40.52 | − 44.75 | − 42.45 |
| $H_s$ (kJ/mol) | | − 45.24 | − 49.58 | − 46.20 |
| $\Delta H$ (kJ/mol) | 6.01 | 4.72(4) | 4.83 | 3.74 |
| $\Delta S$ (J/Kmol) | 22.0 | 18.9 | 19.3 | 16.1 |
| $dp/dT$ (bar/K) | − 137 | − 136 | − 135 | − 130 |

the critical temperature is 521 K.[17] From polarizable models the POL4D has higher melting temperature (260 K) than the BK3, but to achieve this it had to sacrifice the match of lot of other properties, e.g., its dimer energy is low (−23.52 kJ/mol), the densities at high temperatures are too low, and the dielectric constant is higher.[72]

The melting enthalpy of the BK3 model, 4.72 kJ/mol, is lower than the experimental 6.01 kJ/mol. This is the consequence of the low melting point. The BK3 model was fitted to the internal energy of hexagonal ice at 273 K, therefore, the enthalpy difference between the water and ice Ih phases is correct at this temperature, but gets smaller at temperatures below 273 K. The equilibrium ice Ih and water densities and the slope of the equilibrium line at 1 bar are predicted very well both with the BK3 and TIP4P/2005 models.

### G. Ice phases

There are 15 structurally identified polymorphs of ice.[23] The abundance of ice phases is the result of two things. First, the structure of hexagonal ice is perfect to form a complete network of hydrogen bonds, which is necessary to produce the cohesive energy. However, this structure is not very dense, so when the pressure increases the water molecules arrange themselves with more and more dense structures trying to maintain the tetrahedral structure. Second, almost every form besides the proton disordered form has its proton ordered version where the hydrogen bonds of identical crystallographic sites point in the same direction.

TABLE VI. Densities of different ice polymorphs are shown in g/cm$^3$. The experimental data were taken from Ref. 23. The results of the models are calculated by us. The error bar of the calculated densities is ±0.002 g/cm$^3$.

| Ice | $P$ (GPa) | $T$ (K) | Expt. | BK3 | TIP4P/2005 | BKd3 |
|---|---|---|---|---|---|---|
| Ih | 0 | 273 | 0.917 | 0.920 | 0.915 | 0.915 |
| III | 0.28 | 250 | 1.165 | 1.160 | 1.160 | 1.161 |
| VI | 1.18 | 225 | 1.373 | 1.385 | 1.380 | 1.381 |
| VII | 5 | 300 | 1.740 | 1.662 | 1.641 | 1.672 |
| VII | 20 | 300 | 2.143 | 2.051 | 1.957 | 2.032 |

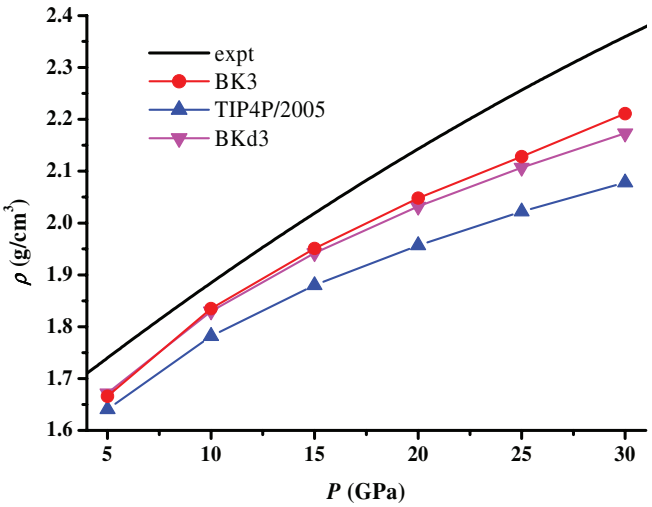


FIG. 15. The density of the ice VII polymorph as a function of pressure at 300 K. The experimental data were taken from Ref. 23. The curves of the models were calculated by us.

A stringent test of the water potentials is how they describe the high-pressure ice phases. Unfortunately, we do not have much calorimetric data, but the structure and density within the range of their stability is known. Therefore, the quality of the model is defined by how accurately the model estimates the density of the given crystals. Note that these properties were not targeted in the fitting procedure of the BK3 model contrary to the TIP4P/2005 which was constructed by exploiting the experience of phase diagram calculations.[6] The results are summarized in Table VI, and the density of the ice VII crystals as function of pressure is shown in Figure 15.

The density of hexagonal ice was a property we had sacrifice for the sake of a better estimation of the self-diffusion coefficient. However, our estimate is still close to the experimental value. The density of the moderately dense ice phases (III and VI) is predicted well by the BK3, TIP4P/2005, and BKd3 models. (The dipole moments of ices Ih, III, VI at the states shown in Table VI are 2.771 D, 2.800 D, and 2.757 D, respectively.) The reasonable good results indicate the abilities of our model, other polarizable models like COS and SWM4 potentials perform poorly in this respect. (See Table IV in Ref. 14.)

Certainly, one cannot expect a perfect estimate of densities in the very high density phase ice VII. This is the crystalline form where, in addition to the 4 hydrogen bonded neighbors, there are 4 contact molecules. As expected, the deformation of the electron cloud of a molecule is more significant, difficult to describe by a simple classical force field. (The dipole moments of ices VII at 10, 20, and 30 GPa are 2.769 D, 2.865 D, and 2.927 D, respectively.) Still, our results are better than the ones of the TIP4P/2005 model.

## VI. CONCLUSIONS

We presented a polarizable model of water capable to give reasonable estimates for many observables all over the entire phase diagram from high pressure crystalline solids

to water clusters. The new model is a result of a systematic search. We studied several of the existing models in the gas phase, liquid phase, and solid phase. As a result, we opted for the best possible combination of model components. The Ewald summation is substantially simpler for charge-on-spring models than for the ones with a polarizable point dipole. Furthermore, Gaussian charge distributions are not just more realistic than point charges, but they also show larger numerical stability against polarization catastrophe. This makes it possible to combine such distributions with the charge-on-spring method and *use only three charges in the model*. The exponential repulsion is also more realistic than the $r^{-12}$ repulsion term of the Lennard-Jones potential and provides better results mainly for gas phase clusters and liquid structure.

Finally, and most importantly, all three charges should take part in the deformation of the charge distribution within the molecule subjected to the polarizing force of the surrounding. It seems that in the absence of a three-dimensional deformation of the charge distribution, polarizable models cannot reproduce the entire temperature-density diagram of water accurately which limits the ability of models to give good predictions to only on one side of this curve. (This is for most polarizable models, the high temperature part is used to obtain a good critical behavior.) These features of the model ensure that with a moderate increase of computational cost (a factor of 4-5 relative to a nonpolarizable model with three point charges) we can estimate the properties of water with a reasonable accuracy.

We tried to find the best possible parametrization of this new model. Obviously, using such a simple description for the water molecule we had to make compromises how accurately certain property should be reproduced. We focused on the ambient liquid properties but at the same time we wanted good results at the two ends of the phase diagram. Our parameterization is not unique but our systematic search indicated that there is no other combination of parameters which could give substantially better overall results for water than the one presented in this paper.

Thus, the new BK3 model gives acceptable estimates over a wide range of thermodynamic states. To the best of our knowledge there is no model, working accurately in such a wide temperature and pressure range, and has overall better performance than BK3 *at the same computational cost.* Our results refer to calculations using Ewald summation. We found this method more reliable than the reaction field. Nevertheless, since the reaction field supposedly provides identical results for the studied properties, this method can also be used in liquid phase, which together with tabulated energies and forces should make it possible to decrease the computational cost.

The simulation code is available from the authors upon request.

## ACKNOWLEDGMENTS

A.B. gratefully acknowledges the support of OTKA Grant No. K84382.

[1] B. Guillot, J. Mol. Liq. **101**, 219 (2002).
[2] M. Chaplin, see http://www.lsbu.ac.uk/water/data.html for the collected experimental data for water.
[3] H. J. C. Berendsen, J. R. Grigera, and T. P. Srtaatsma, J. Phys. Chem. **91**, 6269 (1987).
[4] W. L. Jorgensen, J. Chandrasekhar, J. D. Madura, R. W. Impey, and M. L. Klein, J. Chem. Phys. **79**, 926 (1983).
[5] H. W. Horn, W. C. Swope, J. W. Pitera, J. D. Madura, T. J. Dick, G. L. Hura, and T. Head-Gordon, J. Chem. Phys. **120**, 9665 (2004).
[6] J. L. F. Abascal and C. Vega, J. Chem. Phys. **123**, 234505 (2005).
[7] P. Paricaud, M. Predota, A. A. Chialvo, and P. T. Cummings, J. Chem. Phys. **122**, 244511 (2005).
[8] H. Yu, T. Hansson, and W. F. van Gunsteren, J. Chem. Phys. **118**, 221 (2003).
[9] H. Yu and W. F. van Gunsteren, J. Chem. Phys. **121**, 9549 (2004).
[10] A. P. E. Kunz and W. F. van Gunsteren, J. Phys. Chem. A **113**, 11570 (2009).
[11] G. Lamoureux, A. D. MacKerell, Jr., and B. Roux, J. Chem. Phys. **119**, 5185 (2003).
[12] G. Lamoureux, E. Harder, I. V. Vorobyov, B. Roux, and A. D. MacKerell, Jr., Chem. Phys. Lett. **418**, 245 (2006).
[13] P. T. Kiss and A. Baranyai, J. Chem. Phys. **137**, 084506 (2012).
[14] P. T. Kiss, P. Bertsyk, and A. Baranyai, J. Chem. Phys. **137**, 194102 (2012).
[15] P. T. Kiss and A. Baranyai, J. Chem. Phys. **137**, 194103 (2012).
[16] J. L. F. Abascal and C. Vega, Phys. Rev. Lett. **98**, 237801 (2007).
[17] C. Vega and J. L. F. Abascal, Phys. Chem. Chem. Phys. **13**, 19663 (2011).
[18] J. Yin and D. P. Landau, J. Chem. Phys. **134**, 074501 (2011).
[19] K. M. Benjamin, A. J. Schultz, and D. A. Kofke, J. Phys. Chem. C **111**, 16021 (2007).
[20] K. M. Benjamin, A. J. Schultz, and D. A. Kofke, J. Phys. Chem. B **113**, 7810 (2009).
[21] W. S. Benedict, N. Gailar, and E. K. Plyer, J. Chem. Phys. **24**, 1139 (1956).
[22] H. J. C. Berendsen, J. P. M. Postma, W. F. van Gunsteren, and J. Hermans, in *Intermolecular Forces*, edited by B. Pullmann (Reidel, Dordrecht, 1981).
[23] V. F. Petrenko and R. W. Withworth, *Physics of Ice* (Oxford University Press, New York, 1999).
[24] G. Czakó, E. Mátyus, and A. G. Császár, J. Phys. Chem. A **113**, 11665 (2009).
[25] H. L. Lemberg and F. H. Stillinger, J. Chem. Phys. **62**, 1677 (1975).
[26] A. Rahman, F. H. Stillinger, and F. Lemberg, J. Chem. Phys. **63**, 5223 (1975).
[27] P. Bopp, G. Jancsó, and K. Heinzinger, Chem. Phys. Lett. **98**, 129 (1983).
[28] K. Toukan and A. Rahman, Phys. Rev. B **31**, 2643 (1985).
[29] M. A. Gonzáles and J. L. F. Abascal, J. Chem. Phys. **135**, 224516 (2011).
[30] I. G. Tironi, R. M. Brunne, and W. F. van Gunsteren, Chem. Phys. Lett. **250**, 19 (1996).
[31] S. Habershon, T. E. Markland, and D. E. Manolopoulos, J. Chem. Phys. **131**, 024501 (2009).
[32] F. Paesani, S. Iuchi, and G. A. Voth, J. Chem. Phys. **127**, 074506 (2007).
[33] G. S. Fanourgakis and S. S. Xantheas, J. Chem. Phys. **128**, 074506 (2008).
[34] P. T. Kiss and A. Baranyai, J. Chem. Phys. **131**, 204310 (2009).
[35] N. Pugliano and R. J. Saykally, Science **257**, 1937 (1992).
[36] S. S. Xantheas and T. H. Dunning, Jr., J. Chem. Phys. **98**, 8037 (1993); S. S. Xantheas, C. J. Burnham, and R. J. Harrison, *ibid.* **116**, 1493 (2002).
[37] P. T. Kiss and A. Baranyai, J. Chem. Phys. **134**, 054106 (2011).
[38] A. Rahman and F. H. Stillinger, J. Chem. Phys. **55**, 3336 (1971).
[39] M. W. Mahoney and W. L. Jorgensen, J. Chem. Phys. **112**, 8910 (2000).
[40] S. W. Rick, J. Chem. Phys. **120**, 6085 (2004).
[41] A. A. Chialvo and P. T. Cummings, Fluid Phase Equlib. **150**, 73 (1998).
[42] T. R. Dyke and J. S. Muenter, J. Chem. Phys. **59**, 3125 (1973).
[43] J. Verhoeven and A. Dymanus, J. Chem. Phys. **52**, 3222 (1970).
[44] J. R. Errington and A. Z. Panagiotopoulos, J. Phys. Chem. B **102**, 7470 (1998).
[45] D. E. Williams and S. R. Cox, Acta Crystallogr. B **40**, 404 (1984).
[46] A. Baranyai and T. R. Welberry, Mol. Phys. **73**, 1317 (1991).
[47] N. H. March and M. P. Tosi, *Coulomb Liquids* (Academic Press, London, 1984).
[48] A. Baranyai, I. Ruff, and R. L. McGreevy, J. Phys. C **19**, 453 (1986).
[49] F. J. Vesely, J. Comput. Phys. **24**, 361 (1977).
[50] F. H. Stillinger and C. W. David, J. Chem. Phys. **69**, 1473 (1978).
[51] P. Barnes, J. L. Finney, J. D. Nicholas, and J. E. Quinn, Nature (London) **282**, 459 (1979).
[52] A. Warshel, J. Phys. Chem. **83**, 1640 (1979).
[53] M. Sprik and M. L. Klein, J. Chem. Phys. **89**, 7556 (1988).

[54]T. P. Straatsma and J. A. McCammon, Mol. Simul. **5**, 1881 (1990).
[55]P. Ahlström, A. Wallqvist, S. Engström, and B. Jönsson, Mol. Phys. **68**, 563 (1989).
[56]S. W. Rick, S. J. Stuart, and B. J. Berne, J. Chem. Phys. **101**, 6141 (1994).
[57]J. Brodholt, M. Sampoli, and R. Vallauri, Mol. Phys. **86**, 149 (1995).
[58]J. M. Svishchev, P. G. Kusalik, J. Wang, and R. J. Boyd, J. Chem. Phys. **105**, 4742 (1996).
[59]L. X. Dang and T. M. Chang, J. Chem. Phys. **106**, 8149 (1997).
[60]W. F. Murphy, J. Chem. Phys. **67**, 5877 (1997).
[61]A. Baranyai and P. T. Kiss, J. Chem. Phys. **133**, 144109 (2010).
[62]P. T. Kiss, M. Darvas, A. Baranyai, and P. Jedlovszky, J. Chem. Phys. **136**, 111470 (2012).
[63]A. Baranyai and P. T. Kiss, J. Chem. Phys. **135**, 234110 (2010).
[64]B. Schropp and P. Tavan, J. Phys. Chem. B **112**, 6233 (2008); **114**, 2051 (2010).
[65]M. P. Allen and D. J. Tildesley, *Computer Simulation of Liquids* (Oxford University Press, Oxford, 1987).
[66]M. J. Louwerse and E. J. Baerends, Chem. Phys. Lett. **421**, 138 (2006).
[67]P. T. Kiss and A. Baranyai, J. Chem. Phys. **136**, 104109 (2012).
[68]G. J. Martyna, M. E. Tuckerman, D. J. Tobias, and M. L. Klein, Mol. Phys. **87**, 1117 (1996).
[69]D. Rozmanov and P. G. Kusalik, Phys. Rev. E **81**, 56706 (2010).
[70]I.-C. Yeh and G. Hummer, J. Phys. Chem. B **108**, 15873 (2004).
[71]C. J. Tainter, P. A. Pieniazek, Y.-S. Lin, and J. L. Skinner, J. Chem. Phys. **134**, 184501 (2011).
[72]L. Viererblová and J. Kolafa, Phys. Chem. Chem. Phys. **131**, 19925 (2011).
[73]O. Gereben and L. Pusztai, J. Mol. Liq. **161**, 36 (2011).
[74]S. Tazi, A. Botan, M. Salanne, V. Marry, P. Turq, and B. Rotenberg, J. Phys.: Condens. Matter **24**, 284117 (2012).
[75]W. Yu, P. E. M. Lopes, B. Roux, and A. D. MacKerell, J. Chem. Phys. **138**, 034508 (2013).
[76]Y. Guissani and B. Guillot, J. Chem. Phys. **98**, 8221 (1993).
[77]C. Vega, M. M. Conde, C. McBride, J. L. Abascal, E. G. Noya, R. Ramirez, and L. M. Ses, J. Chem. Phys. **132**, 046101 (2010).
[78]J. Alejandre, D. J. Tildesley, and G. A. Chapela, J. Chem. Phys. **102**, 4574 (1995).
[79]M. Ley-Koo and M. S. Green, Phys. Rev. A **23**, 2650 (1981).
[80]F. J. Wegner, Phys. Rev. B **5**, 4529 (1972).
[81]J. Alejandre, D. J. Tildesley, and G. A. Chapela, Mol. Phys. **85**, 651 (1995).
[82]J. L. Rivera, F. W. Starr, P. Paricaud, and P. T. Cummings, J. Chem. Phys. **125**, 094712 (2006).
[83]C. Vega and E. De Miguel, J. Chem. Phys. **126**, 154707 (2007).
[84]A. Halkier, H. Koch, P. Jorgensen, O. Christiansen, I. M. Beck Nielsen, and T. Helgaker, Theor. Chem. Acc. **97**, 150 (1997).
[85]L. A. Curtiss, D. J. Frurip, and M. Blander, J. Chem. Phys. **71**, 2703 (1979); J. A. Odutola and T. R. Dyke, *ibid.* **72**, 5062 (1980).
[86]J. O. Hirschfelder, C. F. Curtiss, and R. B. Bird, *Molecular Theory of Gases and Liquids* (Wiley, New York, 1954).
[87]F. Sokolic, Y. Guissani, and G. Baranovic, Chem. Phys. Lett. **131**, 513 (1986).
[88]C. Vega, E. Sanz, J. L. F. Abascal, and E. G. Noya, J. Phys. Condens. Matter **20**, 153101 (2008).
[89]R. G. Fernandez, J. L. F. Abascal, and C. Vega, J. Chem. Phys. **124**, 144506 (2006).
[90]C. Vega, M. Martin-Conde, and A. Patrykiejew, Mol. Phys. **104**, 3583 (2006).
[91]A. K. Soper, Chem. Phys. **258**, 121 (2000).